4.1 Introduction

Gels come under a special class of responsive molecular materials that are highly significant due to their wide range of applications in laboratories as well as industries[1]. The various properties can be incorporated into gels such as conductance[2][3], optical[4],[5], rheological[6], morphological, magnetic, catalytic, etc[7]. A viscoelastic gel-like matrix that contains at least one metallic element is a class of metallogel[8]. However, the research in designing novel and precise molecular-level network gel formation has been an inspiring project among scientists. The 3D-interconnected network structure of metallogel can be achieved by vigilant selection of particular ligands and metal ions in a particular solvent such as water, methanol, ethanol, carbon tetrachloride, toluene, acetonitrile, N, N-dimethyl formamide, 1,2 dichlorobenzene, dimethyl sulfoxide, acetone, tetrahydrofuran, etc.[9] Nowadays, the ability to design a metallogel with the ideal properties for a particular purpose turns out to be very challenging and interesting in the scientific community. The immobilization of metal and ligands into a gel is a purely non-covalent interaction. The unique metal-ligand interactions like $n \rightarrow \pi^*$ or $\pi \rightarrow \pi^*$ or hydrogen bonding or hydrophobic interaction[10] are the most prominent driving forces for the stable gel network formation which immobilize large solvent volumes using various mechanisms[11],[12],[13]. Gel matrices are easy to use in several areas including catalysis[14], drug delivery, sensor science[15] medical diagnostics[16], photolithography, cosmetics[17], and biological purposes[18],[19].

Recently, the spacious application of metallogels has been utilized in opto-electronic, and electrical devices[20]. Among them, experiments involving MS-based Schottky barrier diodes (SBDs) have drawn a great deal of attention over the last few years. In almost every semiconductor electronic and optoelectronic device, a metal-semiconducting interface plays a

crucial role in the performance of the devices due to its significant impact on charge flow and electric potential energy[21],[22]. The interface feature is mainly overseen by the Schottky barrier (SB), when a metal is brought into contact with a semiconductor, a barrier forms at the metal-semiconductor interface[5]. The Schottky barrier formation process is well known to depend on interfacial states as defects or metal-induced gap states[23].

In this present effort, we report a supramolecular trimesic acid (TMA) copper (II) based metallogel (Cu-TMA). The semiconducting properties of synthesized metallogel were examined and thus able to create a thin-film device (Ag/Cu-TMA) based on a metal-semiconductor junction at room temperature. In the thin-film Ag/Cu-TMA device, has a remarkable rectification ratio (I_{on}/I_{off}) of ~216 which is very good to that of previously testified literature[24],[25], and the I-*V* characteristics demonstrate a nonlinear rectifying behaviour, suggesting the formation of Schottky Barrier diodes[26],[27],[28]. In-depth research has also shown that the developed Schottky diode based on Ag/Cu-TMA thin film has advantages in terms of improved electrical conductivity, chemical stability, and an inexpensive manufacturing procedure.

4.2 Experimental

4.2.1 Materials

The TMA (95% pure) was procured from S.D. Fine Private Ltd. and metal salts copper acetate monohydrate (98% pure) used throughout the whole experiment were purchased from Sigma-Aldrich, India. The solvents methanol (99% pure), ethanol (99.5% pure), toluene (99% pure), carbon tetrachloride (99.5 % pure) were procured from Sigma-Aldrich, India. All the chemicals were utilised without further purification during the whole work.

4.2.2 Characterization

The UV-vis absorption spectra were recorded on Thermo Scientific EVOLUTION 201 spectrophotometer. The FT-IR characterization has been performed using a PerkinElmer Spectrum spectrophotometer. MS Micromass Technology to capture the HR-MS spectra, a SCIEX X500R QTOF was employed. The Tecnai G2 20 TWIN was used to collect the TEM images. On the Anton Paar MCR 702 Twin Drive Rheometer, metallogel's rheology was accomplished. The EVO-Scanning Electron Microscope MA15/18 was conducted to capture the SEM micrographs. The powder XRD spectrum was recorded on the Rigaku Mini Flex 600 Detector D-tex ultra in the range of $2\theta = 10\text{-}60^{o}$.

4.2.3 Synthesis of Cu -TMA based metallogel

During an experiment involving Cu-TMA metallogel synthesis, 0.199 g copper (II) acetate monohydrate and 0.210 g trimesic acid (1 mmol) were dissolved separately in DMF solvent (1 mL) at room temperature. In a vial-shaped glass container, the blurred DMF solutions of trimesic acid and the blue DMF solutions of copper (II) acetate monohydrate were quickly combined to form a dense greenish-blue combination after dynamic trembling, allowing the mixture to rest for ten minutes, a stable Cu-TMA metallogel with a greenish-blue colour formed. The Cu-TMA metallogel can be kept at ambient temperature for several months in the exposed environment.

4.2.4 Device fabrication

For the fabrication of (MS) junction Schottky barrier diode, indium-doped tin oxide (ITO) coated glass substrates with thickness ~1.1 mm and resistivity ~15-20 (ohm. cm) were cut into small regular square-shaped (15×15 mm^2) using a diamond cutter. The small ITO glass

substrate piece was cleaned thoroughly at first, cleaned the ITO coated glass substrates were in an ultrasonic cleaning bath in a 5% soap solution to remove dust particles for 15 min., then deionized (DI) water with a resistivity of ~18 (MΩ.cm) to get rid of chemical residues for 15 min., then acetone (C_3H_6O) to remove the organic remnants/contaminants from the substrate for 15 min, at last, cleaned by isopropanol (C_3H_8O) for 10 minutes to remove organic residues left on the substrate. Then, the plasma cleaning treatment is applied over substrates for 15 minutes in the presence of oxygen and argon to increase the hydrophilicity of ITO-coated glass substrate[29],[30] In the first deposition step, deposited the supramolecular Cu-TMA-based metallogel solution on the as cleaned ITO coated glass substrate by the spin coating unit (TSE, Model SPM-150LC, Germany) at 1500 rpm for 30 s. The process was optimized and repeated two times (at the same speed and duration) to obtain a supramolecular Cu-TMA-based metallogel layer thickness of ~100 nm. supramolecular Cu-TMA-based metallogel coated ITO samples were then annealed at 100°C for 30 minutes in a muffle furnace[31]. For contact electrode formation, Ag (99.99%) metal dots of ~2 mm diameter (device area 0.0314 cm^2) and ~80 nm thickness were fabricated on the Cu-TMA based metallogel by thermal evaporation unit (Model No. FL400, SMART COAT 3.0 A, Hind High Vacuum India) with the shadow mask technique[32]. The vacuum level was maintained in the range of 10^{-6} mbar with a deposition rate of 0.02 Å/s in the thermal evaporation unit. In the fabricated diode Ag electrode and ITO Substrate have worked as the Upper electrode and Bottom electrode for electrical measurements. The thickness of Cu-TMA-based metallogel layers was measured using the optical spectrometer commonly known as F20-UV, thin-film analyzer (Model No. SDT2, Filmetrics USA) instrument.

4.3 Result and discussion

The Cu-TMA-based mettalogel was synthesized by using copper acetate mono hydrate and trimesic acid for the fabrication of the Schottky Diode, as shown in **Scheme-1**.

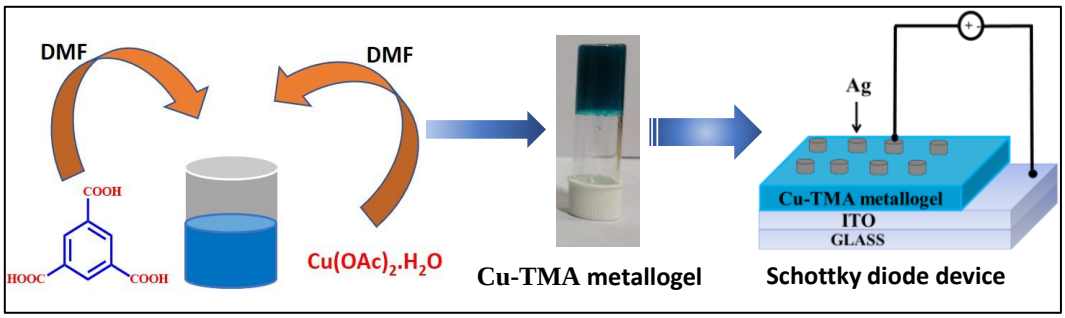

Scheme 4.1 Synthetic scheme for Cu-TMA metallogel and their application towards the fabrication of Schottky Diode

4.3.1. Evaluation of critical gelation concentration

Different metal cations in the "+2" oxidation state, including Cd, Co, Zn, Cu, Ni, Pb, Mn, Fe, and Sn, were added to the TMA gelator in DMF to test the gelation ability. It is worth noting that $Cu(OAc)_2.H_2O$ was the only metal cation that could create a gel with the gelator TMA. An assessment of the Cu-TMA metallogel minimum critical gel concentration in the range of (50-200 mg mL^{-1}) concerning the combined weight of metal and gelator, as depicted in **Figure 4.1** [33]. The ratio of $[Cu(CH_3COO)_2.H_2O]$ to [TMA] in the metallogel-forming ingredients was kept at 1:1 (w/w). The Cu-TMA metallogel was successfully produced by the use of trimesic acid and Cu(II)-acetate salt in DMF solvent at a concentration of 200 mg mL^{-1}

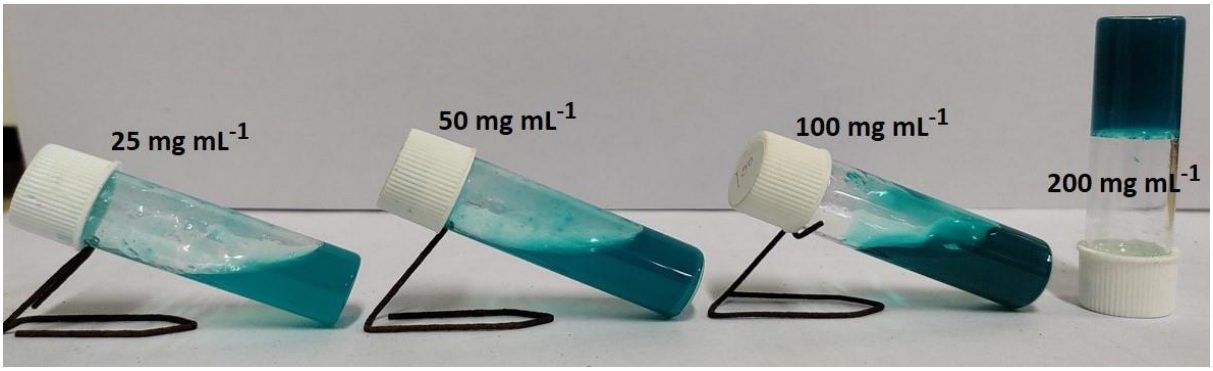

Figure 4.1 The metallogel was found to be 200 mg mL^{-1} concerning the combined weight of $Cu(CH_3COO)_2{\cdot}H_2O$ and trimesic acid.

4.3.2. UV-vis study

The behaviour of the TMA gelator with copper acetate monohydrate in DMF was observed by an analysis using UV-vis absorption spectroscopy**.** We passed out a titration experiment between the gelator (TMA) and Cu (II) metal ion **(Figure 4.2).** A colourless clear solution of

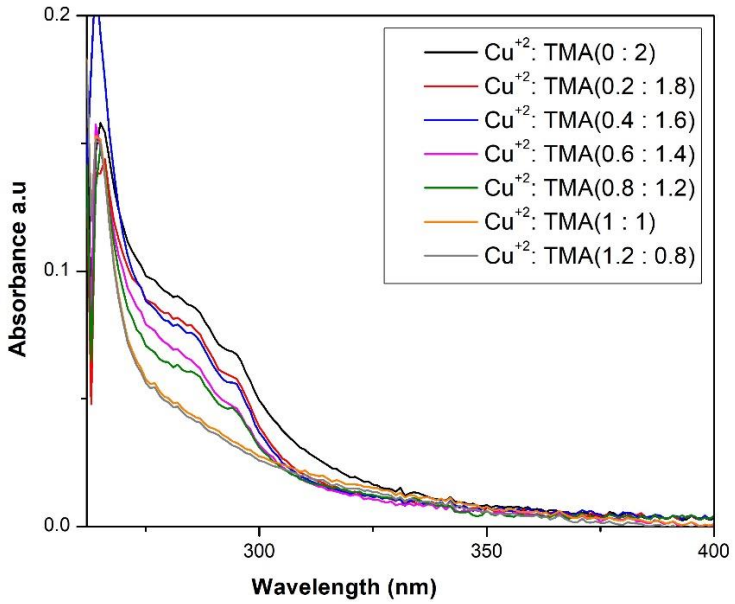

Figure 4.2 UV-visible titration evaluation of TMA ($1x10^{-4}$ M, DMF) with copper (II) acetate monohydrate ($1x10^{-4}$ M, DMF).

gelator (TMA) ($1x10^{-4}$ M, DMF, 25°C) existing a broadband 295 nm consistent to n-π* transition[34][35], after multiple additions of $Cu(OAc)_2$ ($1x10^{-4}$M, DMF 25°C), the band at 295 nm vanished enlightening that the Cu^{+2} had formed a complex with the gelator. The gelator/Cu(II) equivalent has a saturation point reveales the feasibility of 1:1 co-ordination.

4.3.3 FT-IR analysis

The infrared spectral study also visualized several supramolecular interactions. Based on the different FT-IR spectral patterns of the Cu-TMA xerogel and ligand TMA **(Figure 3.3)**, it is evident that there is a substantial shift of FT-IR peak positions of the Cu-TMA metallogel with respect to the FT-IR patterns of trimesic acid, which indicated that trimesic acid interacts with copper acetate monohydrate via n → π* or π → π* interaction. Some significant

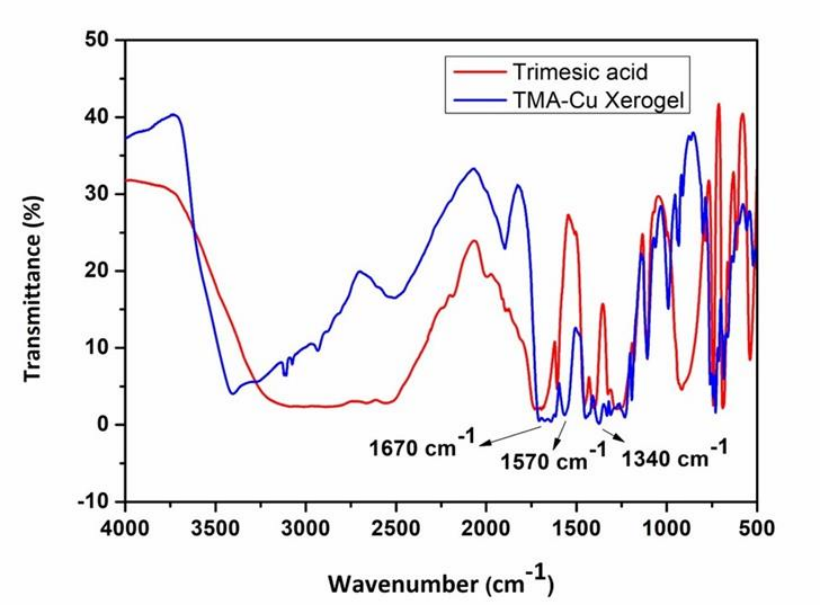

Figure.4.3 FT-IR analysis of Cu-TMA xerogel along with gelator TMA

FTIR peaks for trimesic acid were positioned at (ν_{CO}) 1705 cm^{-1} and (ν_{COO}) 1600 cm^{-1}, 1380 cm^{-1} which corresponds to the asymmetric and symmetric stretching band[36][37]. In addition,

after metallation (ν_{CO}) band shifted to 1670 cm^{-1} and (ν_{COO}) band shifted to 1570 cm^{-1}, 1340 cm^{-1}, respectively.

4.3.4 Morphological study

By using field emission scanning electron microscopy (FE-SEM) and transmission electron microscopy (TEM), the microstructure of a vacuum-dried xerogel (MH-Li) was examined (**Figure 4.4)**. The results confirmed a 3D-interconnected nano-fibrous network, these nanofibrous networks are responsible for the entrapment of the solvent molecules, and consequently the formation of Cu-TMA metallogel. It is possible that the Cu(II) source in DMF and the gelator TMA may interact supramolecularly noncovalently to form a Cu-TMA based stable metallogel by self-assembly. This result exposed that a network of nanofibers was found to be interwoven within this structure with an average diameter of 50 nanometers and micrometres in length[38],[39]. The powder X-ray diffraction pattern of Cu-TMA xerogel revealed a broad peak in the 2θ range of 10^{o} to 80^{o} at 35° and 65° demonstrating the amorphous behaviour of the gel[3] [40],[41]**(Figure 4.5)**. Thermogravimetric analysis of xerogel **(Figure 4.6)** reveals that up to 230°C the overall weight loss was 15%, and temperatures within this range were likely due to the removal of coordinated water molecules per unit formula of metallogel. Further, we observed a prominent weight loss of up to 40% in the temperature range 230°C – 400°C, this stage indicates long-range thermal stability[42],[43]. It also evidences toward the gel melting temperature T_d ~230°C. The molecular ion (m/z) peak observed for Cu-TMA metallogel at m/z 409.7 **(Figure 4.7)** This result of the HR-MS spectrum is corresponding with the calculated peak.

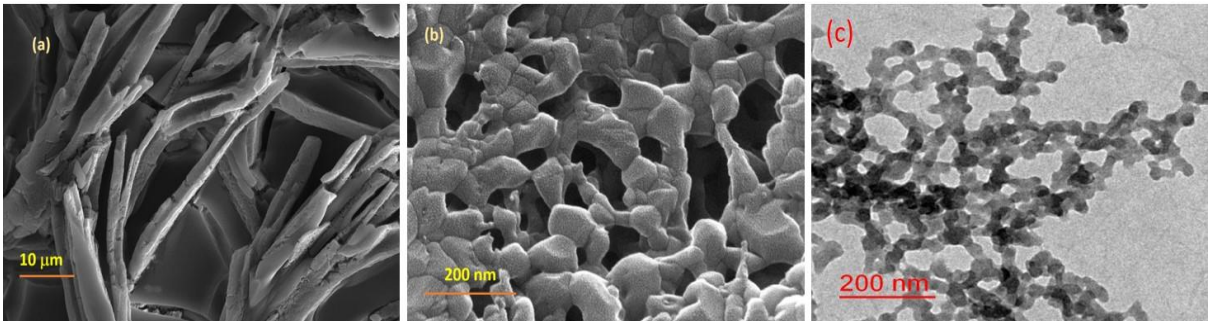

Figure 4.4 (a, b) SEM image of vacuum-dried metallogel and, (c) TEM images of (Cu-TMA; ~10^{-3} M) metallogel, respectively.

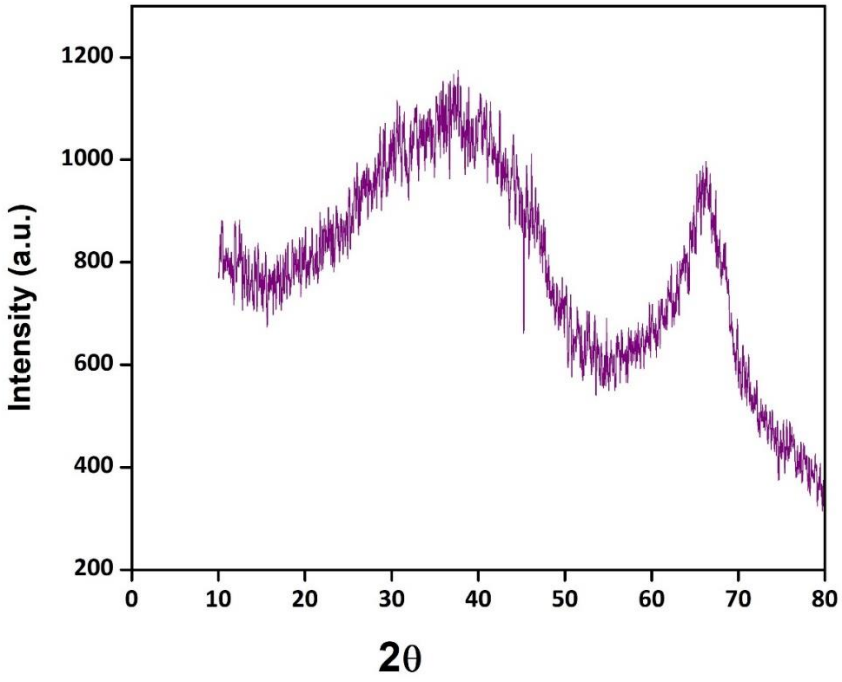

Figure 4.5 PXRD pattern of xerogel indicating amorphous behaviour of Cu-TMA metallogel.

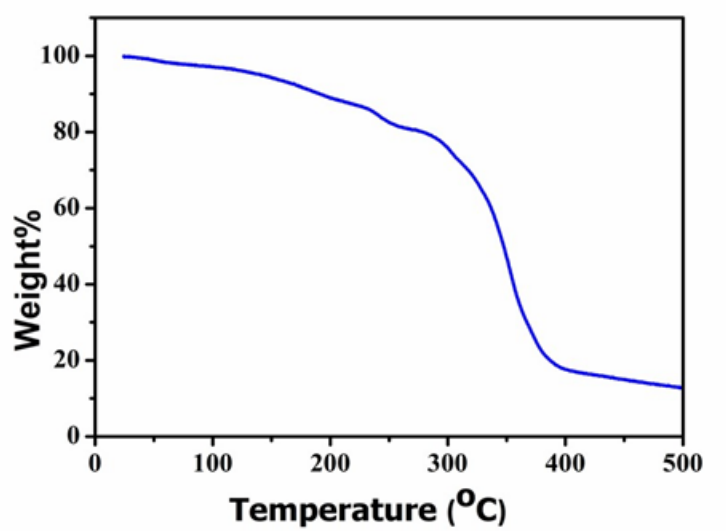

Figure 4.6 Thermogravimetric analysis curve for Cu-TMA Xerogel

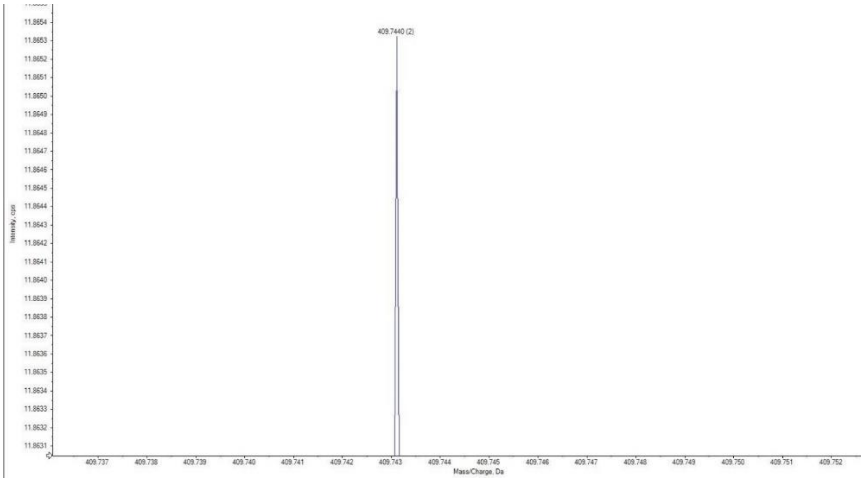

Figure 4.7 HR-MS spectra of Cu-TMA metallogel represent the experimental isotopic abundance pattern for 1:1 TMA vs Cu^{2+}.

4.3.5 Rheological analysis

The interrelation between force and deformation of the matter is described by a rheological experiment. The storage modulus (G′) and loss modulus (G″) are used to illustrate the gel strength, and the frequency-independent G′ is greater than the G″ in the gel state[25].

Throughout the rheological experiments of Cu-TMA metallogel it has been observed that G' is greater than G" by order of one of shear stress at a fixed gel concentration **(Figure 4.8)**. Additionally, we have seen that the gel is destroyed at the point of intersection of G' and G"' at 2.007 Pa shear stress values, which is also known as the gel-sol transition point The dynamic frequency sweep experiment was conducted between 0.1 to 100 rad.s^{-1}. Here, we observe that G′ and G″ are essentially completely independent of frequency changes in a large linear viscoelastic region. Rheological explorations revealed the elastic nature of the gel, and Cu-TMA metallogel satisfies the required essential criteria to establish as a mechanically stable gel material[24].

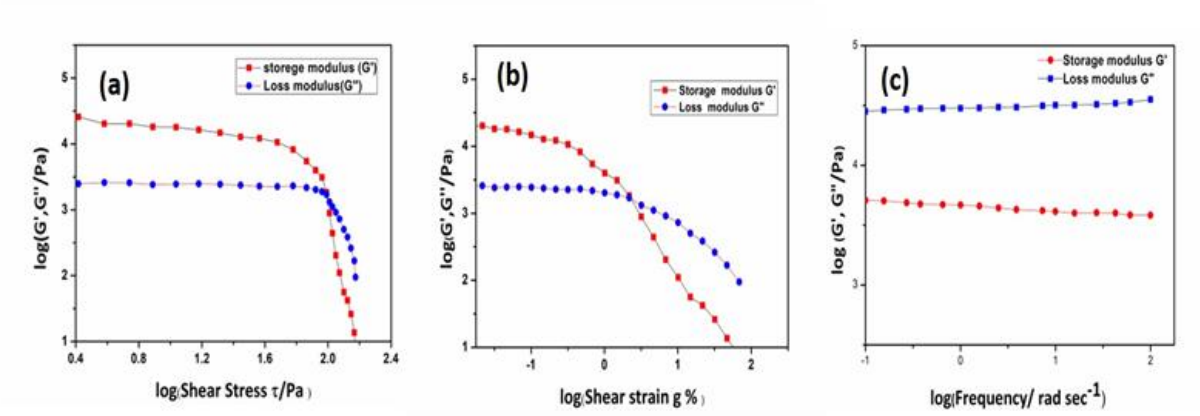

Figure 4.8 (a) Dynamic shear stress against G" and G′, (b) dynamic oscillation Strain vs G" and G′, (c) frequency sweep measurements of G" and G′.

4.3.6 Optical characterization

UV-vis spectroscopy was used to examine the optical properties. The Spectral measurements of thin film (Cu-TMA metallogel) were taken within the wavelength range of 250-600 nm. Utilizing Tauc's equation for thin-film Cu-TMA metallogel, we have calculated the optical band gap[44] **(Figure 4.9)**.

$$(\alpha h\nu)^2 = A(h\nu - E_g)$$

Where, α, h, ν, and Eg represent the absorption coefficient, Planck's constant, light frequency, and the optical bandgap, respectively. 'A' is constant and in an ideal case, its value is unity. The (Eg) for Cu-TMA metallogel was calculated by extrapolating the linear section of the plot $(\alpha h\nu)^2$ vs hν to α = 0 absorptions, and its value obtained was 3.5 eV for Cu-TMA metallogel.

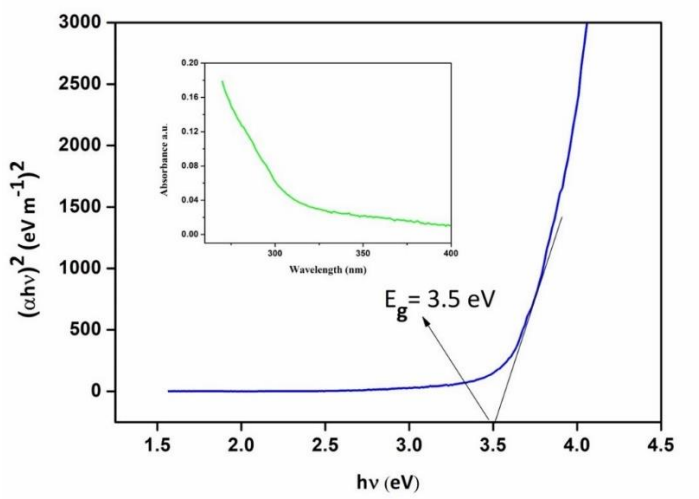

Figure 4.9 Bandgap measurement by Tauc's plot and UV-visible absorption spectrum (**inset**) for Cu-TMA metallogel.

4.3.7. Strategy of device fabrication

A Schottky barrier diode was designed with the help of the aforementioned optical properties of as-synthesised metallogel in **Scheme 1**.

Tauc's plot analysis **(Figure 4.9)** shows that as-synthesized organometallogel (Cu-TMA) falls into the semiconducting-range material category[45],[46]. As a result, we have fabricated a metal (Ag)-Semiconductor (Cu-TMA) (MS) junction-based Schottky barrier diode, a thin-film device and explored its current-voltage (I-V) characteristics. The (*I-V*) measurements of an organo-metallogel (Cu-TMA) based thin-film device were performed at room temperature

using a Semiconductor parameter analyser (B1500A from Keysight, USA) at a bias voltage from -2 V to +2 V. The current was found to be -0.37 A with a reverse bias of 2 V and 80 A with a forward bias of 2 V. The rectification ratio (I_{on}/I_{off}) of the Cu-TMA-based SBD at 2 V was ~ 220, revealing superior for a lately developed device. Further, we have examined the *I-V* characteristics of the Ag/Cu-TMA-based thin-film device (**Figure 4.10)**. The results revealed a nonlinear rectifying behaviour of the interface between Ag/Cu-TMA, indicating the formation of an SBD.

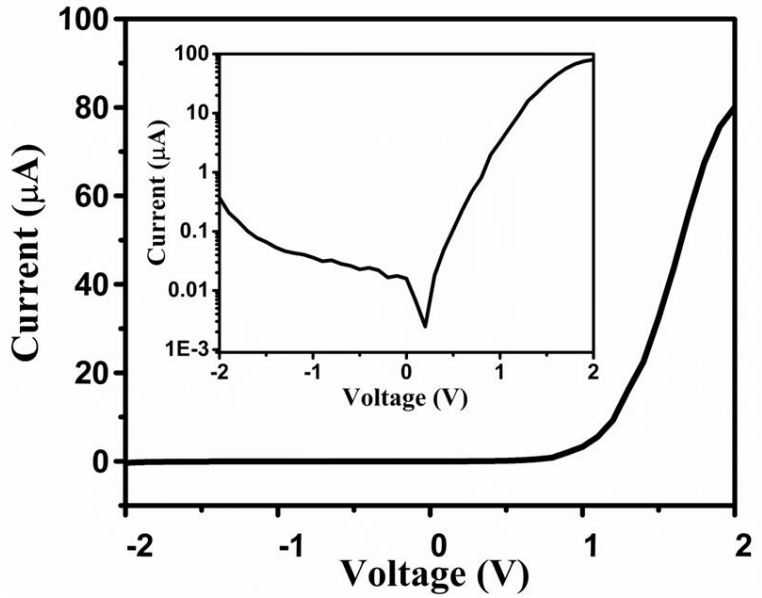

Figure 4.10 *I–V* characteristics graph for ITO/Cu-TMA/Ag-structured thin-film device.

Table4.1 Comparison table of parameters rectification ratio of the Ag/Cu-TMA device

Device name	**Rectification ratio**	**Reference**
Mn@OX/Al	34.50	Biswajit Dey *et al*
$[Cd_4L_2(NCO)_6]_n$	12.44	Hossain *et.al*
$C_{40}H_{34}Cu_2N_6O_{18}$	8.46	S. Dhibar *et.al*
Co-TA/Al	19.27	A.Day *et.al*
Ag/Cu-TMA	**216**	**Present work**

4.4 Conclusion

The novel modular and functional metallogel we have synthesized here is based on trimesic acid and $Cu(OAc)_2.H_2O$ in DMF, and it was developed using a viable synthesis method. The mechanical stability and confirmation of its gel phase were both demonstrated by rheological studies. SEM and TEM investigation indicated that the supramolecular Cu-TMA-based metallogel contains a clearly defined 3D- interconnected nano-fibrous network. The mechanism of metallogel was established by UV-vis, FT-IR, and ESI-MS analysis. By measuring the optical band gap of Cu-TMA metallogel, it was found that the substance possesses a semiconductive nature. Furthermore, we have developed an MS junction thin-film electronic device by using Ag metal and semiconducting Cu-TMA metallogel. The *I–V* characteristics indicate the formation of a Schottky Barrier Diode. Thus, the current study on

ITO/Cu-TMA/Ag advocates the future advanced applications of gelatinous smart materials and their suitability for use in conductive devices and battery electrolytes.

4.5 References

[1] V. Kumar, R. K. Upadhyay, D. Bano, S. Chandra, D. Kumar, S. Jit, S. H. Hasan, *New J. Chem.* **2021**, *45*, 6273–6280.

[2] K. Asadi, F. Gholamrezaie, E. C. P. Smits, P. W. M. Blom, B. De Boer, *J. Mater. Chem.* **2007**, *17*, 1947–1953.

[3] K. Sel, S. Demirci, E. Meydan, S. Yildiz, O. F. Ozturk, H. Al-Lohedan, N. Sahiner, *J. Electron. Mater.* **2015**, *44*, 136–143.

[4] A. Dey, S. Middya, R. Jana, M. Das, J. Datta, A. Layek, P. P. Ray, *J. Mater. Sci. Mater. Electron.* **2016**, *27*, 6325–6335.

[5] K. Parto, A. Pal, T. Chavan, K. Agashiwala, C. H. Yeh, W. Cao, K. Banerjee, *Phys. Rev. Appl.* **2021**, *15*, 1–17.

[6] A. Sallee, K. Ghebreyessus, *Dalt. Trans.* **2020**, *49*, 10441–10451.

[7] S. Dhibar, A. Dey, A. Dey, S. Majumdar, D. Ghosh, P. P. Ray, B. Dey, *ACS Appl. Electron. Mater.* **2019**, *1*, 1899–1908.

[8] P. Ghorai, A. Dey, P. Brandão, J. Ortega-Castro, A. Bauza, A. Frontera, P. P. Ray, A. Saha, *Dalt. Trans.* **2017**, *46*, 13531–13543.

[9] S. Majumdar, S. Sil, R. Sahu, M. Ghosh, G. Lepcha, A. Dey, S. Mandal, P. Pratim Ray, B. Dey, *J. Mol. Liq.* **2021**, *338*, 116769.

[10] A. Sebastian, M. K. Mahato, E. Prasad, *Soft Matter* **2019**, *15*, 3407–3417.

[11] X. Chen, Y. Zhou, M. Yang, J. Wang, C. Guo, Y. Wang, *J. Mol. Struct.* **2022**, *1250*,

131810.

[12] G. Liu, J. Sheng, W. L. Teo, G. Yang, H. Wu, Y. Li, Y. Zhao, *J. Am. Chem. Soc.* **2018**, *140*, 16275–16283.

[13] Y. Kumar, M. Dubey, *Chem. Commun.* **2022**, *58*, 549–552.

[14] J. H. Lee, S. Kang, J. Y. Lee, J. H. Jung, *Soft Matter* **2012**, *8*, 6557–6563.

[15] Y. An, H. Yoshida, Y. Jing, T. Liang, H. Okuzaki, **2022**, DOI 10.1039/d2sm00515h.

[16] J. Jagur-Grodzinski, *Polym. Adv. Technol.* **2010**, *21*, 27–47.

[17] K. Eshun, Q. He, *Crit. Rev. Food Sci. Nutr.* **2004**, *44*, 91–96.

[18] C. Noè, M. Zanon, A. Arencibia, M. J. López-Muñoz, N. F. de Paz, P. Calza, M. Sangermano, *Polymers (Basel).* **2022**, *14*, DOI 10.3390/polym14061268.

[19] P. Raghu, B. E. Kumara Swamy, T. Madhusudana Reddy, B. N. Chandrashekar, K. Reddaiah, *Bioelectrochemistry* **2012**, *83*, 19–24.

[20] A. A. Puranik, P. S. Salunke, N. D. Kulkarni, *New J. Chem.* **2019**, *43*, 14720–17727.

[21] R. T. Tung, *Appl. Phys. Rev.* **2014**, *1*, DOI 10.1063/1.4858400.

[22] P. Rana, R. P. Chauhan, *J. Mater. Sci. Mater. Electron.* **2014**, *25*, 5630–5637.

[23] Z. Zhang, Y. Guo, J. Robertson, *J. Phys. Chem. C* **2020**, *124*, 19698–19703.

[24] S. Dhibar, A. Dey, A. Dey, S. Majumdar, D. Ghosh, P. P. Ray, B. Dey, *ACS Appl. Electron. Mater.* **2019**, *1*, 1899–1908.

[25] A. Dey, S. Sil, S. Majumdar, R. Sahu, M. Ghosh, G. Lepcha, P. Pratim, B. Dey, **2022**, *160*, 1–8.

[26] S. Majumdar, B. Pal, R. Sahu, K. S. Das, P. P. Ray, B. Dey, *Dalt. Trans.* **2022**, 9007–9016.

[27] M. Hussain, S. Aftab, S. H. A. Jaffery, A. Ali, S. Hussain, D. N. Cong, R. Akhtar, Y.

Seo, J. Eom, P. Gautam, H. Noh, J. Jung, *Sci. Rep.* **2020**, *10*, 1–8.

[28] H. Sheng, S. Muthukumar, N. W. Emanetoglu, Y. Lu, *Appl. Phys. Lett.* **2002**, *80*, 2132–2134.

[29] R. K. Upadhyay, **2020**, 2020–2023.

[30] R. K. Upadhyay, A. P. Singh, D. Upadhyay, S. Ratan, C. Kumar, S. Jit, *IEEE Photonics Technol. Lett.* **2019**, *31*, 1151–1154.

[31] S. K. Cheung, N. W. Cheung, *Appl. Phys. Lett.* **1986**, *49*, 85–87.

[32] R. K. Upadhyay, A. P. Singh, D. Upadhyay, A. Kumar, C. Kumar, S. Jit, *IEEE Electron Device Lett.* **2019**, *40*, 1961–1964.

[33] S. Dhibar, A. Dey, S. Majumdar, P. P. Ray, B. Dey, *Int. J. Energy Res.* **2020**, 1–14.

[34] H. F. Abd El-Halim, G. G. Mohamed, E. A. M. Khalil, *J. Mol. Struct.* **2017**, *1146*, 153–163.

[35] J. Díaz-Visurraga, C. Daza, C. Pozo, A. Becerra, C. von Plessing, A. García, *Int. J. Nanomedicine* **2012**, *7*, 3597–3612.

[36] Y. Liu, L. Liu, L. Zhang, X. Lv, G. Che, *Colloids Surfaces A Physicochem. Eng. Asp.* **2020**, *584*, 124053.

[37] W. Zhang, Z. Wang, L. Tao, K. Duan, H. Wang, J. Zhang, X. Pan, Z. Huo, *J. Solid State Electrochem.* **2019**, 1563–1570.

[38] M. Wang, K. Wang, C. Wang, M. Huang, X. Q. Hao, M. Z. Shen, G. Q. Shi, Z. Zhang, B. Song, A. Cisneros, M. P. Song, B. Xu, X. Li, *J. Am. Chem. Soc.* **2016**, *138*, 9258–9268.

[39] T. Xiao, W. Zhong, L. Qi, J. Gu, X. Feng, Y. Yin, Z. Y. Li, X. Q. Sun, M. Cheng, L. Wang, *Polym. Chem.* **2019**, *10*, 3342–3350.

[40] D. Bano, S. Chandra, P. K. Yadav, V. K. Singh, S. H. Hasan, *J. Photochem. Photobiol. A Chem.* **2020**, *398*, 112558.

[41] B. S. Luisi, K. D. Rowland, B. Moulton, *Chem. Commun.* **2007**, 2802–2804.

[42] F. Rezaei, R. Yunus, N. A. Ibrahim, *Mater. Des.* **2009**, *30*, 260–263.

[43] N. DiFonzo, P. Bordia, *J. Allergy Clin. Immunol.* **1998**, *130*, 556.

[44] S. Dhibar, A. Dey, S. Majumdar, D. Ghosh, A. Mandal, P. P. Ray, B. Dey, *Dalt. Trans.* **2018**, *47*, 17412–17420.

[45] F. Davar, M. Mohammadikish, M. Reza Loghman-Estarki, Z. Hamidi, *CrystEngComm* **2012**, *14*, 7338–7344.

[46] P. K. Yadav, R. K. Upadhyay, D. Kumar, D. Bano, S. Chandra, S. Jit, S. H. Hasan, *New J. Chem.* **2021**, *45*, 12549–12556.